Scattering of reorientational optical solitary waves at dielectric perturbations

Alessandro Alberucci,[1] Gaetano Assanto,[1] Antonmaria A. Minzoni,[2] and Noel F. Smyth[3]

[1]*NooEL-Nonlinear Optics and OptoElectronics Lab, University of Rome "Roma Tre," Via della Vasca Navale 84, IT-00146 Rome, Italy*

[2]*Fenomenos Nonlineales y Mecánica (FENOMEC), Department of Mathematics and Mechanics, Instituto de Investigación en Matemáticas Aplicádas y Sistemas, Universidad Nacional Autónoma de México, 01000 México, Distrito Federal, Mexico*

[3]*School of Mathematics and Maxwell Institute for Mathematical Sciences, University of Edinburgh, Edinburgh EH9 3JZ, Scotland, United Kingdom*

(Received 29 April 2011; published 4 January 2012)

We discuss the interaction of spatial solitary waves in nematic liquid crystals, termed nematicons, with localized inhomogeneities in the distribution of the optic axis. For beam waists small compared with the defect width, self-localization is preserved; in the opposite limit the spatial solitary waves undergo significant attenuation due to diffractive losses, to the extent that nematicons are essentially destroyed. Owing to their power-waist dependence spatial solitary waves interacting with defects in nematic liquid crystals are subject to an excitation-dependent transition from particlelike to wavelike behavior. In the latter regime their trajectory varies with input power, leading to novel approaches to the design and realization of all-optical circuits.

DOI: 10.1103/PhysRevA.85.013804 PACS number(s): 42.65.Tg, 42.70.Df, 05.45.Yv

I. INTRODUCTION

Since the early days of nonlinear optics, self-localization of light in space has been among the most intriguing phenomena in the field [1–3]. The first studies on beam self-trapping were carried out in focusing Kerr media, for which the nonlinear variations in refractive index (Δn) are proportional to the local intensity I; that is, $\Delta n = n_2 I$ [2,3]. Hence, a bell-shaped propagating beam can induce a dielectric channel waveguide able to confine it, as well as low power probes, even at different wavelengths [4,5]. Such a transversely localized beam, that is, a bright spatial solitary wave in which diffraction and self-focusing mutually balance can therefore be considered a mode of the self-induced waveguide [6].

In the paraxial approximation nonlinear light localization in propagating wave packets is governed by the generalized nonlinear Schrödinger equation (NLSE)

$$2ik_0 n_0 \frac{\partial A}{\partial z} + \frac{\partial^2 A}{\partial x^2} + \frac{\partial^2 A}{\partial y^2} + 2n_0 k_0^2 \Delta n(|A|^2)A = 0, \quad (1)$$

where A is the slowly varying scalar field envelope, z is the propagation coordinate, x and y are the coordinates transverse to this, n_0 is the carrier refractive index, and $I \propto |A|^2$. It should be noted that Eq. (1) is not limited to optics, but can describe nonlinear propagation in several contexts, from plasmas [7] to fluid dynamics [8], Bose-Einstein condensates [9], etc. In pure Kerr media, for which $\Delta n = n_2 I$, two-dimensional (2D) solitary wave solutions stemming from Eq. (1) are unstable and subject to filamentation and catastrophic collapse [4]. 2D solitary waves can be stabilized in cubic media by eliminating diffraction in one direction [10,11] or by resorting to additional, higher-order effects in order to modify the character of $\Delta n(I)$, for instance a dependence on higher powers of I, that is, $\Delta n = n_2 I + n_4 I^2 + n_6 I^3 + \cdots$ [12], index saturation [13], multiphoton absorption [14], or nonlocality, that is, an all-optical response extending beyond the transverse size of the light beam [15–18].

To date, spatial optical solitary waves have been observed in several bulk materials, including atomic vapors [19], high-polarizability glasses [20,21], air [22], photorefractives [23], and nematic liquid crystals (NLCs) [24,25]. Two-color stable solitary waves have also been obtained via a parametric nonlinearity, for example, via second harmonic generation [26–28]. The possibility of guiding and controlling light by light is fascinating from a theoretical perspective [29], as well as toward the implementation of all-optical signal processing schemes [30]. Both aspects have been investigated in the past decade in a NLC, which features a large nonlinearity and can support solitary waves, often called nematicons [25], at powers of milliwatts [24,31], or even lower in the presence of dopants [32–34]. The response of a NLC is also highly nonlocal; that is, the width of Δn is much larger than the beam waist [18,35,36], allowing a drastic simplification of their modeling at variance with standard (local) Kerr media [29]. The highly nonlocal response allows long-range interactions between nematicons [37], enabling the realization of all-optical logic gates and power-controlled beam routers [38–40]. The scattering of solitary waves by photonic potentials has been investigated in purely Kerr media, both experimentally [41] and theoretically or numerically [42–45]. In a NLC the giant reorientational response allows the dielectric tensor to be easily perturbed by electric fields [46], leading to nematicon steering via voltage [47,48], deflection via interactions with localized defects [49–51], as well as with interfaces [52–55].

In previous studies of nematicon scattering by perturbations, however, the self-trapped intensity profile was assumed substantially narrower than the defect width; that is, the corresponding dielectric tensor did not change appreciably across the solitary profile [40,49]. In this limit the beam evolves according to geometric optics and behaves as a particle, that is, the solitary wave retains its character of a highly peaked distribution in space and its trajectory does not depend on its waist [50,51,55]. In this paper, conversely, we discuss, both theoretically and numerically, nematicon interactions with a (wide) defect which strongly modulates the beam phase front, taking into account the role of diffraction and nonlocality in the scattering process.

II. MODULATION THEORY

Let us consider a NLC layer in a planar cell. A voltage across the cell thickness [24,31] or rubbing of the glass-NLC interfaces [33,39,47,53,56–60] can be employed to pretilt the main axis of the organic molecules $\hat{\theta}$ (i.e., the optic axis or director) in the plane xz, avoiding the Freédericksz threshold to reorientation by extraordinary waves propagating with an electric field polarized along x. The coordinate system is defined with z as the distance down the cell (or propagation coordinate) and (x,y) orthogonal to this, with the (x,z) the principal plane containing both the optic axis and the wave vector of the extraordinary beam. An additional localized reorientation θ_b above the pretilt $\hat{\theta}$ can introduce a localized refractive index perturbation, that is, a defect, in the cell. A number of physical mechanisms can result in such a defect, including static or low-frequency electric fields [40,50,61] and finite light beams [53]. A nematicon is a light beam of envelope E_n and with polarization in the (x,z) plane, of power large enough to cause a nonlinear reorientation θ_n of the NLC director. In the usual limit of a small additional reorientation as compared to the pretilt, the nondimensional equations governing the propagation of the solitary wave, or nematicon, in the medium are [18,35,51,62]

$$i\frac{\partial E_n}{\partial z} + i\Delta'\theta_b\frac{\partial E_n}{\partial x} + \frac{1}{2}\nabla^2 E_n + 2E_n(\theta_n + \theta_b) = 0, \tag{2}$$

$$\nu\nabla^2\theta_n - 2q\theta_n = -2|E_n|^2, \tag{3}$$

The parameter ν measures the strength of the elastic response of the material; that is, it quantifies the nonlocality of the response. In most experimental situations ν is large, $O(100)$ [63], and NLC is said to be highly nonlocal. The parameter q is related to the effective pretilt of the optic axis, due to either an applied voltage across x (q proportional to the square of the pretilting field) or molecular anchoring in the plane yz (q related to the cell thickness [36]). The inherent birefringent walkoff $\Delta(\theta)$ of the Poynting vector of extraordinary waves has been expanded in a Taylor series about the pretilt

$$\Delta = \Delta(\hat{\theta}) + \Delta'(\hat{\theta})\theta_b + \cdots, \tag{4}$$

assuming that $|\theta_b| \ll |\hat{\theta}|$ (and the reorientation θ_n due to the nematicon) is smaller than that defining the defect. Moreover, the uniform walkoff due to the pretilt $\Delta(\hat{\theta})$ has been factored out by a phase transformation in E_n. It should be emphasized that the nematicon equations (2) and (3) are generic, with the present results qualitatively valid even in the $(1+1)$-dimensional simplification of Eqs. (2) and (3) [36].

There are no known exact solutions of the NLC equations (2) and (3), in particular, no exact solitary wave solutions. Approximate solutions obtained by modulation theory [8] have been found to yield results in good agreement with both numerical and experimental findings [63–66]. Since modulation theory has already been employed to describe similar problems of beam refraction due to index changes in a NLC [51], for the sake of clarity the actual modulation equations used in the present work are given in Appendix A, and only the specific details concerning beam evolution and refraction or scattering due to interactions with defects will be highlighted here. The modulation theory is based on assuming the trial functions

$$\begin{aligned} E_n &= af(\rho_e)e^{i\sigma+iV(x-\xi)} + ige^{i\sigma+iV(x-\xi)}, \\ \theta_n &= \alpha f^2(\rho_n), \end{aligned} \tag{5}$$

for the nematicon and director response [51], respectively, where

$$\rho_e = \frac{\sqrt{(x-\xi)^2+y^2}}{w}, \quad \rho_n = \frac{\sqrt{(x-\xi)^2+y^2}}{\beta}. \tag{6}$$

Here a and w are the amplitude and waist of the nematicon, α and β are the amplitude and width of the director response, σ is the propagation constant, ξ is the position of the nematicon peak, and V is the angle of propagation of the nematicon in the (z,x) plane. The parameter g gives the amplitude of the low-wave-number diffractive radiation which accumulates under the nematicon as it evolves [67]. This shelf exists in the circular region $0 \leqslant (x-\xi)^2 + y^2 \leqslant \ell^2$ centered on the solitary wave [64]. In many situations, a nematicon's trajectory is largely independent of its profile f [50,65]. Popular choices for this profile are a Gaussian $f(\rho) = \exp(-\rho^2)$ and a hyperbolic secant $f(\rho) = \operatorname{sech}\rho$. The modulation equations given in Appendix A are left in a general form valid for any reasonable choice of f for which the integrals given in Appendix B exist and for any refractive index defect θ_b. In the present work, a hyperbolic secant profile will be used.

The modulation equations of Appendix A show that the effect of a refractive index defect on the nematicon trajectory is encompassed by the modulation equations

$$\frac{d}{dz}(S_2a^2w^2 + \Lambda g^2)V = S_2a^2w^2(2-\Delta'V)F_\xi, \tag{7}$$

$$\frac{d\xi}{dz} = V + \Delta'F. \tag{8}$$

The first of these is the momentum equation for the nematicon and the second is the equation for the beam path when walkoff is included. The term F determines the effect of the defect on the nematicon trajectory and is given by the integral

$$F = \frac{\int_{-\infty}^{\infty}\int_{-\infty}^{\infty}\theta_b(x,z)f^2(x,y)\,dxdy}{\int_{-\infty}^{\infty}\int_{-\infty}^{\infty}f^2(x,y)\,dxdy}. \tag{9}$$

This integral gives an averaged effect of the spatially varying index change over the nematicon profile. When the nematicon waist is much smaller than the defect size, θ_b in the numerator of F can be approximated by its value at the nematicon peak and $F = \theta_b(\xi,z)$. The conservation of momentum equation (7), providing the soliton trajectory, can then be approximated by

$$\frac{dV}{dz} = (2-\Delta'V)\frac{\partial\theta_b}{\partial\xi}. \tag{10}$$

The nematicon trajectory is given by this equation for conservation of momentum and Eq. (8) for the beam's path and is thus independent of the solitary wave profile f [51]. However, in the present work we shall also be interested in the limit in which the nematicon is much wider than the defect. In that case F, given by (9), needs to be evaluated exactly and the nematicon trajectory will no longer be independent of its profile.

Let us assume that the optic axis distribution due to the defect has the Gaussian profile

$$\theta_b = a_b e^{-[(x-X_b)^2+(z-Z_b)^2]/w_b^2}. \tag{11}$$

As the nematicon trajectory will depend on its profile, let us consider the profile $f(\rho) = \operatorname{sech}\rho$ for E_n in the trial function (5). The effect of the defect on the trajectory is therefore given by

$$F = \frac{a_b w_b}{\sqrt{B^2 w^2 + w_b^2}} e^{-(z-Z_b)^2/w_b^2-(\xi-X_b)^2/(B^2w^2+w_b^2)}, \tag{12}$$

on using (9), with the constant B given in Appendix B. In the limit $w \ll w_b$ (nematicon waist w much smaller than the defect width), F is independent of w, in agreement with previous work [51] and the result $F = \theta_b(\xi,z)$ discussed above.

III. LINEAR THEORY

Before considering the nonlinear equations (2) and (3), it is instructive to tackle the linear refraction problem described by the linearized version of the electric field equation (2)

$$i\frac{\partial E_n}{\partial z} + \frac{1}{2}\nabla^2 E_n + 2\theta_b E_n = 0. \tag{13}$$

This linearized equation can be solved in the WKB, or geometric optics, approximation for each ray impinging on the defect. Unfortunately, such ray equations cannot be solved for the Gaussian defect profile (11). We therefore approximate the Gaussian defect (11) in the limit of a wide defect, so that w_b is large, by

$$\theta_b = n_D\left[1 - w_b^{-2}(x^2+z^2)\right], \tag{14}$$

where $n_D = a_b$ is the maximum refractive index jump within the defect relative to the constant index of refraction n_1 external to the defect. For convenience, the defect is centered at the origin instead of (X_b, Z_b). In the limit $w_b \gg 1$ the ray trajectories inside the defect, given by the phase integral, can be approximated by straight lines parallel to the z axis. Therefore, the total phase is a linear function of z and the WKB solution takes the form

$$Ae^{2in_D z}, \tag{15}$$

with a constant amplitude A. Defining φ as the polar angle measured from the center of the defect, the WKB solution at the edge of the defect is

$$Ae^{2in_D \sin\varphi}. \tag{16}$$

To construct the WKB solution outside the defect, Huygen's principle can be used to calculate the phase at the observation point (x,z); since the index of refraction n_1 outside the defect is constant, the rays from the edge of the defect to the observation point (x,z) travel in straight lines. Therefore, the final WKB solution has the form

$$Ar^{-1/2}e^{i\Psi(\varphi,x,z)}, \tag{17}$$

where the phase Ψ is determined by the initial value $n_D \sin\varphi$ added to the optical path between the defect and the observation point. The factor $r^{-1/2}$ is the usual geometric decay factor, with r the distance between the observation point and the end point of the internal ray with polar angle φ. This gives

$$\Psi(\varphi,x,z) = 2n_D\left[1 - \frac{1}{2}\left(\varphi - \frac{\pi}{2}\right)^2\right] + n_1\sqrt{(x-\cos\varphi)^2 + (z-\sin\varphi)^2}. \tag{18}$$

The total field then results from the superposition

$$E_n(x,z) = \int_0^\pi A(\varphi)e^{i\Psi(\varphi,x,z)}\,d\varphi. \tag{19}$$

This expression gives the full asymptotic solution for the wave (Helmholtz) equation governing the linear beam. It contains the asymptotic solution of the wave equation in the parabolic approximation (13).

The main point of interest of the WKB solution (19) is that a caustic can form. Since the cusp of the caustic forms in the region around $\varphi = \pi/2$, let us expand the phase Ψ locally in this region and set $\zeta = \varphi - \pi/2$. Then for small $|\zeta|$

$$\Psi(\zeta,x,z) = n_D + n_1 + n_1 z - n_D\zeta^2 + \frac{n_1}{2}\left(x^2 - 2x\zeta - \frac{1}{6}x\zeta^3 + z^2 + 2z\zeta^2\right). \tag{20}$$

Notice that the $n_1 z$ term, which is the phase corresponding to the carrier wave, is factored out in the parabolic approximation. Thus, the dominant contribution to the field of the envelope in the solution (19) is given by the points of stationary phase $\Psi_\zeta(\zeta,x,z) = 0$, which is an equation for the corresponding ray. The caustic is given by the coalescence of rays, that is, the solution of $\Psi_\zeta(\zeta,x,z) = \Psi_{\zeta\zeta}(\zeta,x,z) = 0$. Solving these equations we find for the caustic

$$z - \frac{n_D}{n_1} = \pm\frac{1}{2}x. \tag{21}$$

The light is concentrated along this caustic, with a shadow region inside its two branches. Note that the expansion (20) limits the validity of the caustic (21) to a small region close to the cusp. Other caustics and higher-order diffraction in the shadow region are not encompassed by the present approximation.

The nonlinear correction to linear caustics has been studied in the slowly varying envelope approximation, leading to NLS-type equations describing spatial solitary waves guided along the caustics [68,69]. Due to the cubic nature of the nonlinearity, there is no field inside the caustic itself. Since a plane wave impinging on the defect was considered for the linearized equations, the nonlinear counterpart is a nematicon impinging on a defect of comparable width. In this limit we expect the nematicon to be stopped at the cusp of the linear caustic and two new beams to appear along the corresponding branches of the linear caustic. If the nematicon does not impinge on the defect at a right angle, the caustics and the nonlinear beams along them are tilted.

Figure 1 shows an example of the solution of the linearized equation (13) for an initial beam impinging orthogonally on the defect and with waist comparable to the defect width. The destruction of the main beam and the resulting caustics can be clearly seen, in accord with the linear theory. Note that the

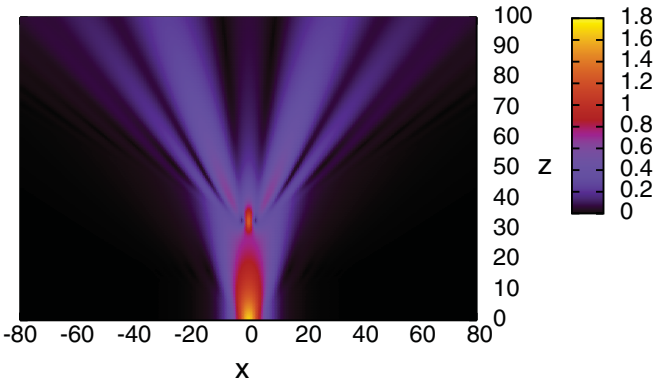

FIG. 1. (Color online) Evolution of $|E_n|$ at $y = 0$ for linearized equation (13). The initial condition is $f(\rho) = \operatorname{sech}\rho$ with (A13), $w = 3.0$, and $\xi = 0.0$. The defect parameters are $a_b = 0.5$, $w_b = 3.0$, $X_b = 0$, and $Z_b = 30$.

approximate solution of the linearized equation recovers the main caustic close to the peak of the defect due to the nature of the expansion. The other lateral caustics visible in the figure are not included in the expansion. Moreover, the bright region of low power inside the caustic region, that is, the shadow zone, is due to higher-order diffraction, as in the penumbria region [70]. This feature is also not captured by the present approximation.

IV. RESULTS

The modulation equations describing the approximate evolution of the nematicon and its trajectory due to the defect are (A1)–(A8) with (12). The solutions of these equations are now compared and combined with full numerical solutions of the NLC equations (2) and (3), obtained using a pseudospectral method [71], to elucidate the dependence of the solitary wave behavior on the relative size of the beam and the defect. In order to isolate the role of this refractive index defect on the nematicon, we chose the initial condition at $z = 0$ to be a steady solitary wave, well approximated using the modulation equations of Appendix A, with (A12)–(A14). Although these steady nematicon relations are approximate, the numerical solution of the NLC equations (2) and (3) shows little amplitude variation when they are used as an initial condition.

Let us first consider a nematicon waist w much smaller than the defect width w_b. Typical examples are illustrated in Fig. 2. The trajectories starting at $\xi = 5,2,0$ show the beam refracting through the defect, with excellent agreement between numerical and modulation trajectories. After going near the center of the defect, the numerical trajectories have some slight oscillation not shown by the modulation trajectories. This is because modulation theory treats the nematicon as a point particle. In reality, however, a nematicon is an extended object subjected to a refractive index gradient across its profile. This results in a distortion of its profile, with an oscillation in its peak position [51]. As the refractive gradient decreases across the nematicon, these oscillations reduce in magnitude [51]. Figure 2(a) shows a typical comparison between the nematicon amplitudes as given by numerical and modulation solutions.

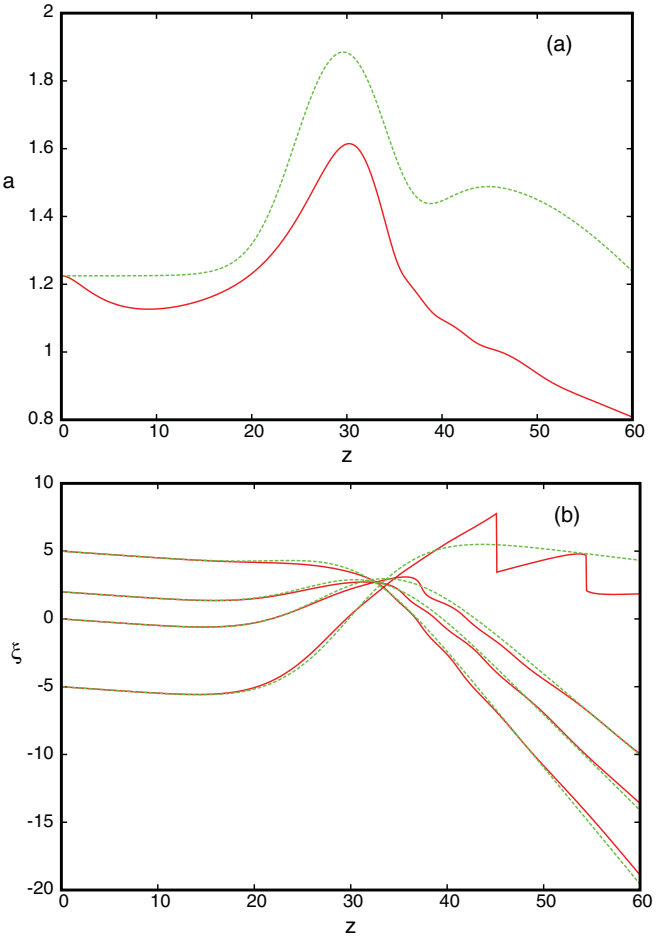

FIG. 2. (Color online) Comparison of numerical and modulation solutions for a wide defect. Numerical solution, full, red line; solution of modulation equations, dashed, green line. The initial condition is $f(\rho) = \operatorname{sech}\rho$, $w = 3.0$, $V = -0.05$, with $\nu = 200$, $q = 2$, and $\Delta' = 1.0$. The defect parameters are $a_b = 0.5$, $w_b = 10.0$, $X_b = 0$, and $Z_b = 30$. (a) Amplitude a for $\xi = 2$ at $z = 0$; (b) positions ξ for initial values $\xi = 5,2,0, -5$.

The nematicon trajectory is generally largely independent of its profile [51,55,72]; hence, the amplitude comparisons for beams starting at $\xi = 5$ and $\xi = 0$ are similar to this comparison for a beam starting at $\xi = 2$. The agreement is good until the beam passes the defect center. Afterward, the beam is distorted, accounting for the differences in amplitude for $z > 40$.

The extended (nonlocal) nature of a nematicon and the resulting variation in refractive index across its profile can have a major effect if the gradient is large enough, as for the beam starting at $\xi = -5$. As visible in Fig. 2(b), the trajectory of this beam starts to zigzag after $z = 40$. In fact, as seen in Fig. 3, the beam is split into three by the defect: The original one decays, to be replaced by a second beam formed from its tail at a larger ξ; this also decays to be replaced by a third one at an even larger ξ. The formation of these two new beams at different ξ explains the two zigzags in Fig. 2(b) as the numerical code computes the position as the maximum of $|E_n|$ at a given z. This evolution is in stark contrast with that of the other beams, an example of which is in Fig. 4. The different

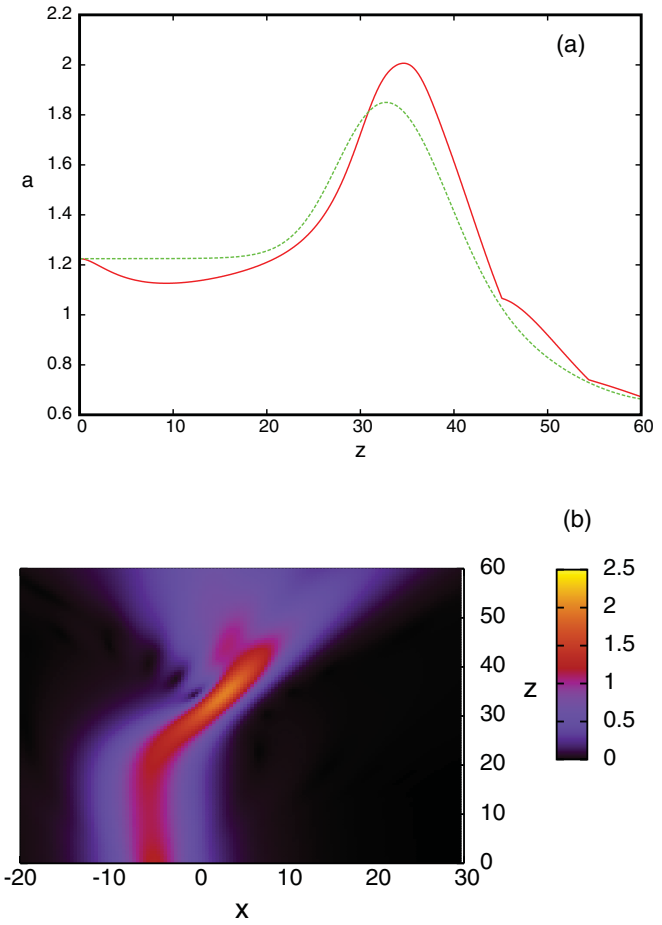

FIG. 3. (Color online) Solutions for initial condition $f(\rho) =$ sech ρ, $w = 3.0$, $V = -0.05$, and $\xi = -5$ with $\nu = 200$, $q = 2$, and $\Delta' = 1.0$. The defect parameters are $a_b = 0.5$, $w_b = 10.0$, $X_b = 0$, and $Z_b = 30$. (a) Amplitude a. Numerical solution, full, red line; modulation solution, (dashed, green line). (b) Evolution of numerical solution $|E_n|$ at $y = 0$.

behavior for the beam starting at $\xi = -5$ can be explained by examining its trajectory in Fig. 2(b). The beam passes through the defect center, unlike the other three; then, it goes through much higher refractive index gradients than the others and suffers much more distortion, enough to split it. The partial

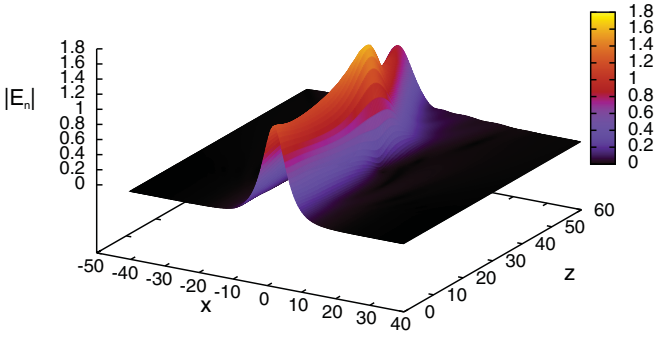

FIG. 4. (Color online) Evolution of $|E_n|$ at $y = 0$. The initial condition is $f(\rho) =$ sech ρ, $w = 3.0$, $V = -0.05$, $\xi = 2.0$, with $\nu = 200$, $q = 2$ and $\Delta' = 1.0$. The defect parameters are $a_b = 0.5$, $w_b = 10.0$, $X_b = 0$, and $Z_b = 30$.

beam destruction is confirmed by the amplitude evolution, shown in Fig. 3(a), with the amplitude being halved. This figure also shows that the amplitude predicted by modulation theory is in excellent agreement with the numerical amplitude, even past $z = 40$, at which the beam splits, a surprising result as the modulation solution assumes a fixed, single-peak nematicon profile.

The beam interaction with and refraction by the defect changes markedly when the beam and defect have comparable widths, as expected from the linear analysis of Sec. III. A typical example is illustrated in Fig. 5. Figure 5(a) displays the amplitude evolution. After leaving the defect central region, both the numerical and the modulation solutions indicate that the beam disintegrates. This can be understood by examining the evolution in position for a variety of launch locations, as in Fig. 5(b). The numerical trajectories exhibit sudden jumps in positions around $z = 35$, with Fig. 5(a) showing a corresponding sudden decrease in amplitude. Figure 6 displays a typical numerical solution for the evolution of $|E_n|$. The destruction of the beam center and the formation of two new beams along the nonlinear caustic are apparent.

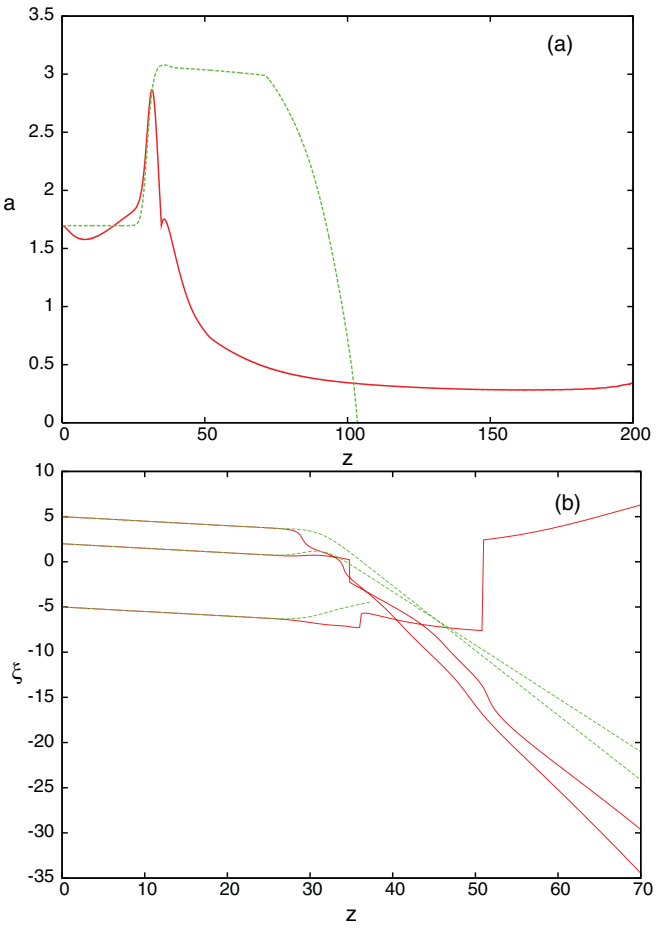

FIG. 5. (Color online) The initial condition is $f(\rho) =$ sech ρ, $w = 3.0$, and $V = -0.05$, with $\nu = 400$, $q = 2$, and $\Delta' = 1.0$. The defect parameters are $a_b = 0.5$, $w_b = 3.0$, $X_b = 0$, and $Z_b = 30$. Numerical solution, full, red line; modulation solution, dashed, green line. (a) Amplitude a for $\xi = 2$ at $z = 0$, (b) positions ξ for initial values $\xi = 5,2,0,-5$.

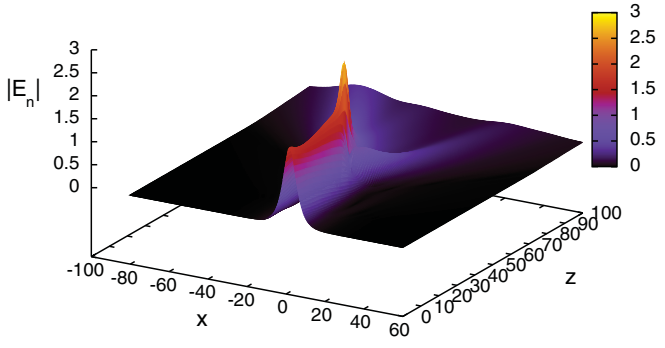

FIG. 6. (Color online) Evolution of $|E_n|$ at $y = 0$. The initial condition is $f(\rho) = \text{sech}\,\rho$, $w = 3.0$, $V = -0.05$, $\xi = 2.0$, with $\nu = 400$, $q = 2$, and $\Delta' = 1.0$. The defect parameters are $a_b = 0.5$, $w_b = 3.0$, $X_b = 0$, and $Z_b = 30$.

This is the nonlinear counterpart of the linear solution in Fig. 1. As the numerical solution tracks the beam position by searching for the maximum $|E_n|$, the trajectory starting at $\xi = 2$ [Fig. 5(b)] after $z = 35$ corresponds to the beam with the largest amplitude. This rapid decay of the beam peak explains the abrupt change in position shown in Fig. 5(b) as the wings of the original beam form two new beams. The modulation equations, in fact, are based on the trial function (5) with a fixed profile. As the beam is destroyed by the defect, good agreement between numerical and modulation solutions is not expected past $z \approx 35$; on the contrary, however, the modulation solution predicts the beam to collapse around $z = 100$, in remarkable agreement with the numerics. Finally, according to the modulation equations the beam starting at $\xi = -5$ dies not long after leaving the defect center.

As the strength a_b of the defect decreases, its effect on the solitary wave becomes less pronounced, as expected. Figure 7 shows amplitude and trajectory comparisons for a defect which has half the amplitude of the cases in Fig. 5, while Fig. 8 shows the nematicon evolution. Clearly, the reduction in beam amplitude on going through the defect is much less and the beam generated along the second branch of the nonlinear caustic has minimal amplitude compared with the main beam propagating into $\xi < 0$, in contrast with the evolution in Fig. 6.

Figures 5(a) and 6 show that the beam tails form new beams of much reduced amplitudes along the nonlinear caustic after the beam peak has been destroyed. This is explored further in Fig. 9 for a larger nonlocality $\nu = 1000$: A nematicon of amplitude about one-third of the initial one is eventually recovered from the beam remnants. As the nonlocality ν increases, both the initial amplitude a (A13) and width of director distribution β (A14) increase. As ν increases there is then more optical power in the portions of the beam away from the defect center. Once this power is large enough, a new nematicon can form. For NLS-type equations a minimum threshold is required before a solitary wave is generated, unlike for Korteweg–de Vries–type equations [73]. For nonlocality ν less than about 200 there is not enough power in the beam tails to form new nematicons along the caustic. For ν above 200 the beam amplitudes along the caustic increase as the nonlocality ν increases. As for the case in Fig. 5, there is surprisingly good

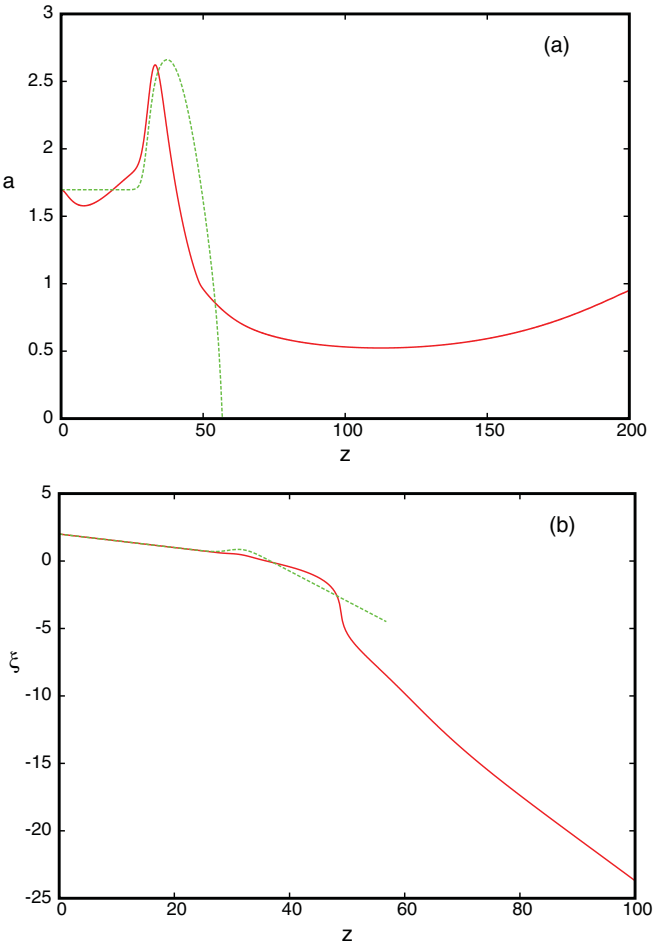

FIG. 7. (Color online) The initial condition is $f(\rho) = \text{sech}\,\rho$, $w = 3.0$, $V = -0.05$, $\xi = 2.0$, with $\nu = 400$, $q = 2$, and $\Delta' = 1.0$. The defect parameters are $a_b = 0.25$, $w_b = 3.0$, $X_b = 0$, and $Z_b = 30$. Numerical solution, full, red line; modulation solution, dashed, green line. (a) Amplitude a, (b) position ξ.

agreement between the numerical and modulation solutions after the point at which the beam breaks apart. The modulation solution predicts the beam to die at about $z = 50$, consistent with the numerics.

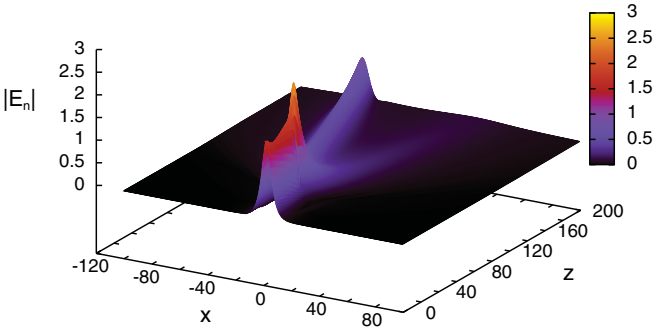

FIG. 8. (Color online) Evolution of $|E_n|$ at $y = 0$. The initial condition is $f(\rho) = \text{sech}\,\rho$, $w = 3.0$, $V = -0.05$, $\xi = 2.0$, with $\nu = 400$, $q = 2$, and $\Delta' = 1.0$. The defect parameters are $a_b = 0.25$, $w_b = 3.0$, $X_b = 0$, and $Z_b = 30$.

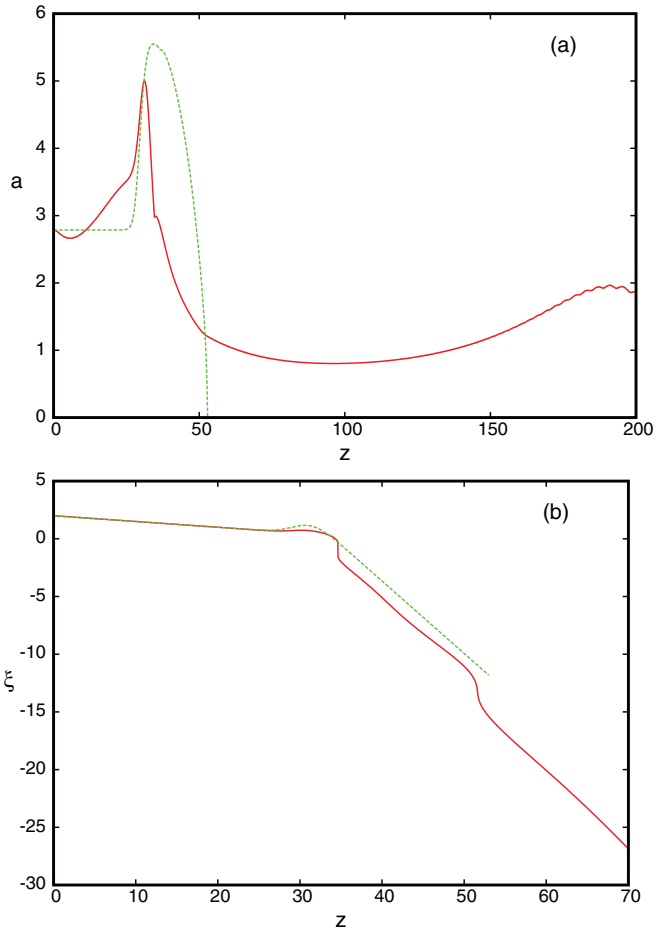

FIG. 9. (Color online) The initial condition is $f(\rho) = \operatorname{sech}\rho$, $w = 3.0$, $V = -0.05$, $\xi = 2.0$, with $\nu = 1000$, $q = 2$, and $\Delta' = 1.0$. The defect parameters are $a_b = 0.5$, $w_b = 3.0$, $X_b = 0$, and $Z_b = 30$. Numerical solution, full, red line; modulation solution, dashed, green line. (a) Amplitude a, (b) position ξ.

V. CONCLUSIONS

The effect of a localized refractive index perturbation on the propagation of a solitary wave in NLCs, a nematicon, has been investigated using both modulation theory and full numerical solutions of the governing equations. Depending on the relative widths of the nematicon and the defect, the nematicon can behave as a particle, propagating according to nonlinear WKB asymptotics [8], or break up and form a nonlinear counterpart to a linear caustic. In the limit in which the defect is much wider than the nematicon, generally the nematicon is simply refracted and undergoes some shape distortion, with excellent agreement between the modulation theory and numerical solutions. However, if the defect is strong enough and the nematicon goes through or near its center, the refractive gradient can tear the solitary wave apart into multiple beams.

A linear WKB analysis has shown that a plane wave incident on a defect is destroyed, with the generation of a caustic consisting of two branches. The nonlinear counterpart of this is a nematicon of waist comparable or larger than the defect width. In this case the nematicon is destroyed and two beams are generated along the nonlinear caustic. The amplitude and existence of these new beams are highly dependent on the nonlocality ν. For a nonlocality ν less than 200 there is not enough optical power to form new nematicons. As ν increases, however, the amplitudes of the new beams grow, because a nematicon's waist increases with ν and so does the optical power in its tails, until it is large enough to form new nematicons. The modulation theory provides good agreement with numerical solutions up to the point where the beam is destroyed and two new beams form.

The modulation theory used shows that the behavior of the beam is controlled by one key function encompassing the beam and its width relative to the defect, F in Eq. (9). This function determines the trajectory of the beam and, depending on the ratio of the beam and defect widths, can be reduced to asymptotic forms relevant to the particle case in which the solitary wave behaves as a particle on propagating through the defect or behaves as a wave and breaks up into nonlinear caustics.

ACKNOWLEDGMENTS

This research was supported by the Royal Society of London under Grant No. JP090179 and in Italy by the Air Force Office of Scientific Research, Air Force Material Command, USAF, under Grant No. FA-8655-10-1-3010.

APPENDIX A: MODULATION EQUATIONS

Substituting the trial functions (5) into a Lagrangian formulation of the NLC equations (2) and (3) [51] results in the modulation equations

$$\frac{d}{dz}(S_2 a^2 w^2 + \Lambda g^2) = -2\delta\tilde{\Lambda}\kappa^2, \tag{A1}$$

$$S_1 \frac{d}{dz} a w^2 = \Lambda g \left(\sigma' - V\xi' + \frac{1}{2}V^2\right), \tag{A2}$$

$$S_1 \frac{dg}{dz} = \frac{S_{22} a}{2w^2} - \frac{A^2 B^4 \alpha a \beta^2 w^2}{(A^2\beta^2 + B^2 w^2)^2} + \frac{1}{2} S_2 a w (2 - \Delta' V) F_w - 2 S_1 \delta g, \tag{A3}$$

$$S_2 \left(\frac{d\sigma}{dz} - V\frac{d\xi}{dz} + \frac{1}{2}V^2\right) = -\frac{S_{22}}{w^2} + \frac{A^2 B^2 \alpha \beta^2 (A^2\beta^2 + 2B^2 w^2)}{(A^2\beta^2 + B^2 w^2)^2} + S_2 (2 - \Delta' V)\left(F - \frac{1}{2} w F_w\right), \tag{A4}$$

$$\frac{d}{dz}(S_2 a^2 w^2 + \Lambda g^2) V = S_2 a^2 w^2 (2 - \Delta' V) F_\xi, \tag{A5}$$

$$\frac{d\xi}{dz} = V + \Delta' F, \tag{A6}$$

and

$$\alpha = \frac{A^2 B^2 \beta^2 a^2 w^2}{2(A^2\beta^2 + B^2 w^2)(2\nu S_{42} + q S_4 \beta^2)}, \tag{A7}$$

$$\alpha = \frac{A^2 B^4 a^2 w^4}{q S_4 (A^2\beta^2 + B^2 w^2)^2}, \tag{A8}$$

for the evolution of the spatial solitary wave in a NLC [51]. The integrals S_i and S_{ij} and the constants A and B are given in Appendix B. Finally, $\Lambda = \ell^2/2$, which is the area of the shelf of radiation under the nematicon, modulo 2π. The actual expression for ℓ is given in [64].

When the beam waist is small in comparison with the defect size, the shed diffractive radiation has little effect on the trajectory [51]. However, when these widths are comparable, including the effect of this radiation is crucial as the beam undergoes significant changes and sheds a large amount of radiation. Therefore, loss has been included in the modulation equations with a coefficient δ [64,66],

$$\delta = \frac{-\sqrt{2\pi}}{32 e \kappa \tilde{\Lambda}} \int_0^z \pi \kappa(z') \ln[(z-z')/\tilde{\Lambda}] \times \left[\left\{ \left[\frac{1}{2} \ln[(z-z')/\tilde{\Lambda}] \right]^2 + \frac{3\pi^2}{4} \right\}^2 + \pi^2 \{\ln[(z-z')/\tilde{\Lambda}]\}^2 \right]^{-1} \frac{dz'}{(z-z')}. \tag{A9}$$

Finally,

$$\kappa^2 = \frac{1}{\tilde{\Lambda}} [S_2 a^2 w^2 - S_2 \hat{a}^2 \hat{w}^2 + \tilde{\Lambda} g^2]. \tag{A10}$$

The caret superscript refers to fixed point values of the quantities, which can be found using energy conservation [64,66]. The parameter $\tilde{\Lambda}$ is the effective point at which the shed diffractive radiation starts [64]. For a stable nematicon, this point is the end of the perturbation of the director due to the beam and is given by [64]

$$\tilde{\Lambda} = \tfrac{1}{2}(7\beta_{1/2})^2, \quad \beta_{1/2} = \beta \,\mathrm{sech}^{-1}(1/\sqrt{2}). \tag{A11}$$

In contrast, when the beam and defect sizes are comparable, radiation has a much greater, indeed controlling, effect and starts at the edge of the beam, so that $\tilde{\Lambda} = \Lambda$.

These modulation equations can be used to approximately find a steady nematicon. Equation (A3) shows that the waist of the steady nematicon is the solution of

$$S_{22} = \frac{2A^2 B^4 \alpha \beta^2 w^4}{(A^2\beta^2 + B^2 w^2)^2}. \tag{A12}$$

Using this steady-state relation, it can be found from the modulation equations (A7) and (A8) that for a given steady nematicon waist w the corresponding steady amplitude is

$$a^2 = \frac{S_{22}(A^2\beta^2 + B^2 w^2)^3 (2\nu S_{42} + q S_4 \beta^2)}{A^4 B^6 \beta^4 w^6}, \tag{A13}$$

with amplitude α of the optic axis distribution given by (A8) and its width given by

$$\beta^2 = \frac{q S_4 B^2 w^2 + \sqrt{q^2 S_4^2 B^4 w^4 + 16 \nu q S_{42} S_4 A^2 B^2 w^2}}{2 q A^2 S_4}. \tag{A14}$$

APPENDIX B: INTEGRALS

The integrals S_i and $S_{i,j}$ in the modulation equations are

$$S_1 = \int_0^\infty \rho f(\rho)\, d\rho, \quad S_2 = \int_0^\infty \rho f^2(\rho)\, d\rho,$$
$$S_{22} = \int_0^\infty \rho \left[\frac{df}{d\rho}\right]^2 d\rho, \quad S_{x32} = \int_0^\infty \rho^3 f^2(\rho)\, d\rho, \tag{B1}$$
$$S_{42} = \frac{1}{4}\int_0^\infty \rho \left[\frac{d}{d\rho} f^2(\rho)\right]^2 d\rho, \quad S_4 = \int_0^\infty \rho f^4(\rho)\, d\rho.$$

For $f(\rho) = \mathrm{sech}\,\rho$,

$$S_1 = 2C, \quad S_2 = \ln 2, \quad S_{22} = \tfrac{1}{3}\ln 2 + \tfrac{1}{6},$$
$$S_{x32} = 1.352\,314\,016\ldots, \tag{B2}$$
$$S_{42} = \tfrac{2}{15}\ln 2 + \tfrac{1}{60}, \quad S_4 = \tfrac{2}{3}\ln 2 - \tfrac{1}{6}.$$

Here C is the Catalan constant $C = 0.915\,965\,594\ldots$ [74]. For $f(\rho) = \exp(-\rho^2)$,

$$S_1 = \tfrac{1}{2}, \quad S_2 = \tfrac{1}{4}, \quad S_{22} = \tfrac{1}{2}, \quad S_{x32} = \tfrac{1}{8},$$
$$S_{42} = \tfrac{1}{8}, \quad S_4 = \tfrac{1}{8}. \tag{B3}$$

The constants A and B arising in the modulation equations are

$$A = \frac{S_2\sqrt{2}}{\sqrt{S_{x32}}} \quad \text{and} \quad B = \sqrt{2S_2}. \tag{B4}$$

[1] V. I. Talanov, Radiophysics **8**, 254 (1964).
[2] R. Y. Chiao, E. Garmire, and C. H. Townes, Phys. Rev. Lett. **13**, 479 (1964).
[3] P. L. Kelley, Phys. Rev. Lett. **15**, 1005 (1965).
[4] Y. S. Kivshar and G. P. Agrawal, Optical Solitons (Academic Press, San Diego, 2003).
[5] C. Conti and G. Assanto, *Encyclopedia of Modern Optics*, Vol. 5 (Elsevier, Oxford, 2004), pp. 43–55.
[6] G. I. Stegeman and M. Segev, Science **286**, 1518 (1999).
[7] K. Ohe and M. Hashimoto, J. Appl. Phys. **58**, 2975 (1985).
[8] G. B. Whitham, *Linear and Nonlinear Waves* (Wiley-Interscience, New York, 1974).
[9] F. Dalfovo, S. Giorgini, L. P. Pitaevskii, and S. Stringari, Rev. Mod. Phys. **71**, 463 (1999).
[10] A. Barthelemy, S. Maneuf, and C. Froehly, Opt. Comm. **55**, 201 (1985).
[11] J. S. Aitchison, A. M. Weiner, Y. Silberberg, M. K. Oliver, J. L. Jackel, D. E. Leaird, E. M. Vogel, and P. W. E. Smith, Opt. Lett. **15**, 471 (1990).
[12] P. Béjot, J. Kasparian, S. Henin, V. Loriot, T. Vieillard, E. Hertz, O. Faucher, B. Lavorel, and J.-P. Wolf, Phys. Rev. Lett. **104**, 103903 (2010).
[13] E. L. Dawes and J. H. Marburger, Phys. Rev. **179**, 862 (1969).
[14] A. Pasquazi, S. Stivala, G. Assanto, J. Gonzalo, and J. Solis, Phys. Rev. A **77**, 043808 (2008).

[15] G. Vitrant, R. Reinisch, J. C. Paumier, G. Assanto, and G. I. Stegeman, Opt. Lett. **14**, 898 (2006).
[16] D. Suter and T. Blasberg, Phys. Rev. A **48**, 4583 (1993).
[17] O. Bang, W. Krolikowski, J. Wyller, and J. J. Rasmussen, Phys. Rev. E **66**, 046619 (2002).
[18] C. Conti, M. Peccianti, and G. Assanto, Phys. Rev. Lett. **91**, 073901 (2003).
[19] J. E. Bjorkholm and A. A. Ashkin, Phys. Rev. Lett. **32**, 129 (1974).
[20] C. Rotschild, O. Cohen, O. Manela, M. Segev, and T. Carmon, Phys. Rev. Lett. **95**, 213904 (2005).
[21] A. Pasquazi, S. Stivala, G. Assanto, J. Gonzalo, J. Solis, and C. N. Afonso, Opt. Lett. **32**, 2103 (2007).
[22] A. Braun, G. Korn, X. Liu, D. Du, J. Squier, and G. Mourou, Opt. Lett. **20**, 73 (1995).
[23] M. Segev, B. Crosignani, A. Yariv, and B. Fischer, Phys. Rev. Lett. **68**, 923 (1992).
[24] G. Assanto and M. Peccianti, IEEE J. Quantum Electron. **39**, 13 (2003).
[25] G. Assanto and M. Karpierz, Liq. Cryst. **36**, 1161 (2009).
[26] W. E. Torruellas, Z. Wang, D. J. Hagan, E. W. VanStryland, G. I. Stegeman, L. Torner, and C. R. Menyuk, Phys. Rev. Lett. **74**, 5036 (1995).
[27] W. E. Torruellas, G. Assanto, B. L. Lawrence, R. A. Fuerst, and G. I. Stegeman, Appl. Phys. Lett. **68**, 1449 (1996).
[28] G. Leo, A. Amoroso, L. Colace, G. Assanto, R. V. Roussev, M. M. Fejer, Opt. Lett. **29**, 1776 (2004).
[29] A. W. Snyder and D. J. Mitchell, Science **276**, 1538 (1997).
[30] G. Stegeman, D. Christodoulides, and M. Segev, IEEE J. Sel. Top. Quantum Electron. **6**, 1419 (2000).
[31] M. Peccianti, G. Assanto, A. De Luca, C. Umeton, and I. C. Khoo, Appl. Phys. Lett. **77**, 7 (2000).
[32] S. V. Serak, N. V. Tabiryan, M. Peccianti, and G. Assanto, IEEE Photonics Technol. Lett. **18**, 1287 (2006).
[33] A. Piccardi, A. Alberucci, and G. Assanto, Phys. Rev. Lett. **104**, 213904 (2010).
[34] A. Piccardi, A. Alberucci, and G. Assanto, Electron. Lett. **46**, 790 (2010).
[35] C. Conti, M. Peccianti, and G. Assanto, Phys. Rev. Lett. **92**, 113902 (2004).
[36] A. Alberucci, A. Piccardi, M. Peccianti, M. Kaczmarek, and G. Assanto, Phys. Rev. A **82**, 023806 (2010).
[37] M. Peccianti and G. Assanto, Opt. Lett. **26**, 1791 (2001).
[38] M. Peccianti, C. Conti, G. Assanto, A. De Luca, and C. Umeton, Appl. Phys. Lett. **81**, 3335 (2002).
[39] A. Fratalocchi, A. Piccardi, M. Peccianti, and G. Assanto, Opt. Lett. **32**, 1447 (2007).
[40] A. Piccardi, A. Alberucci, U. Bortolozzo, S. Residori, and G. Assanto, IEEE Photonics Technol. Lett. **22**, 694 (2010).
[41] Y. Linzon, R. Morandotti, M. Volatier, V. Aimez, R. Ares, and S. Bar-Ad, Phys. Rev. Lett. **99**, 133901 (2007).
[42] X. D. Cao and B. A. Malomed, Phys. Lett. A **206**, 177 (1995).
[43] R. H. Goodman, P. J. Holmes, and M. I. Weinstein, Physica D **192**, 215 (2004).
[44] E. N. Tsoy and C. M. de Sterke, Phys. Lett. A **372**, 1856 (2008).
[45] C. P. Jisha, A. Alberucci, R.-K. Lee, and G. Assanto, Opt. Lett. **36**, 1848 (2011).
[46] F. Simoni, *Nonlinear Optical Properties of Liquid Crystals* (World Scientific, Singapore, 1997).
[47] M. Peccianti, C. Conti, G. Assanto, A. De Luca, and C. Umeton, Nature (London) **432**, 733 (2004).
[48] A. Piccardi, M. Peccianti, G. Assanto, A. Dyadyusha, and M. Kaczmarek, Appl. Phys. Lett. **94**, 091106 (2009).
[49] A. Pasquazi, A. Alberucci, M. Peccianti, and G. Assanto, Appl. Phys. Lett. **87**, 261104 (2005).
[50] A. Alberucci, A. Piccardi, U. Bortolozzo, S. Residori, and G. Assanto, Opt. Lett. **35**, 390 (2010).
[51] G. Assanto, A. A. Minzoni, N. F. Smyth, and A. L. Worthy, Phys. Rev. A **82**, 053843 (2010).
[52] M. Peccianti, A. Dyadyusha, M. Kaczmarek, and G. Assanto, Nat. Phys. **2**, 737 (2006).
[53] A. Piccardi, G. Assanto, L. Lucchetti, and F. Simoni, Appl. Phys. Lett. **93**, 171104 (2008).
[54] Y. V. Izdebskaya, V. G. Shvedov, A. S. Desyatnikov, W. Krolikowski, and Y. S. Kivshar, Opt. Lett. **35**, 1692 (2010).
[55] G. Assanto, B. D. Skuse, and N. F. Smyth, Phys. Rev. A **81**, 063811 (2010).
[56] A. Alberucci, M. Peccianti, G. Assanto, A. Dyadyusha, and M. Kaczmarek, Phys. Rev. Lett. **97**, 153903 (2006).
[57] A. Fratalocchi, A. Piccardi, M. Peccianti, and G. Assanto, Phys. Rev. A **75**, 063835 (2007).
[58] Y. Izdebskaya, V. Shvedov, A. S. Desyatnikov, Y. S. Kivshar, W. Krolikowski, and G. Assanto, J. Eur. Opt. Soc. **5**, 10008 (2008).
[59] A. Piccardi, A. Alberucci, and G. Assanto, Appl. Phys. Lett. **96**, 061105 (2010).
[60] Y. V. Izdebskaya, V. G. Shvedov, A. S. Desyatnikov, W. Z. Krolikowski, M. Belic, G. Assanto, and Y. S. Kivshar, Opt. Express **18**, 3258 (2010).
[61] A. Piccardi, A. Alberucci, U. Bortolozzo, S. Residori, and G. Assanto, Appl. Phys. Lett. **96**, 071104 (2010).
[62] M. Peccianti, A. Fratalocchi, and G. Assanto, Opt. Express **12**, 6524 (2004).
[63] G. Assanto, A. A. Minzoni, M. Peccianti, and N. F. Smyth, Phys. Rev. A **79**, 033837 (2009).
[64] A. A. Minzoni, N. F. Smyth, and A. L. Worthy, J. Opt. Soc. Am. B **24**, 1549 (2007).
[65] B. D. Skuse and N. F. Smyth, Phys. Rev. A **77**, 013817 (2008).
[66] B. D. Skuse and N. F. Smyth, Phys. Rev. A **79**, 063806 (2009).
[67] W. L. Kath and N. F. Smyth, Phys. Rev. E **51**, 1484 (1995).
[68] R. Haberman and R.-J. Sun, Stud. Appl. Math. **72**, 1 (1985).
[69] R. Haberman and D. Allgaier, SIAM J. Appl. Math. **45**, 919 (1985).
[70] M. Kline and I. W. Kay, *Electromagnetic Theory and Geometrical Optics* (Interscience, New York, 1965).
[71] B. Fornberg and G. B. Whitham, Philos. Trans. R. Soc. London A **289**, 373 (1978).
[72] G. Assanto, B. Skuse, and N. Smyth, Photonics Lett. Pol. **1**, 154 (2009).
[73] A. C. Newell, *Solitons in Mathematics and Physics* (SIAM, Philadelphia, 1985).
[74] M. Abramowitz and I. Stegun, *Handbook of Mathematical Functions with Formulas, Graphs and Mathematical Tables* (Dover, New York, 1972).